J Solid State Electrochem (2009) 13:573–582
DOI 10.1007/s10008-008-0664-6

ORIGINAL PAPER

Convolutive reshaping with applications for voltammetry

Peter J. Mahon

Received: 31 July 2008 / Revised: 25 August 2008 / Accepted: 26 August 2008 / Published online: 16 September 2008

Abstract A convolutive procedure is described that enables the current that is due to planar diffusion to be extracted from voltammograms for electrodes where current due to non-planar diffusion is substantial. This transformation enables rapid assessment of the reversibility of an electrochemical reaction based on departures from the well-known behavior that has been widely described for planar diffusion. However, this assessment will not be strictly quantitative in all cases due to restrictions that apply for situations where theoretical descriptions based on convolution integrals arise in electrochemical systems. Five examples are described, which includes spherical, disk, and cylindrical electrodes as well as Nernst diffusion layers with impermeable and open boundaries. A related procedure known as convolutive forecasting that is able to predict the steady-state current from near steady-state voltammograms has been extended so that an exact treatment of the disk electrode is now possible.

Keywords Voltammetry · Convolution · Spherical correction · Convolutive forecasting · Nernst layer · Electrode geometry

Introduction

The ease of interpretation of experimental data is an important factor in the development of an analysis method with familiarity based on knowledge, training, and experience being a powerful tool during the initial evaluation of any recorded results. Expert users of voltammetry can readily detect the influence of processes such as diffusion, adsorption, and irreversibility when scrutinizing their data based on any disparity between what they have observed and what they expect for a particular set of experimental conditions. For casual users or novices, knowledge obtained from 'textbook' examples could be the limit of their experience, or indeed interest, of voltammetry with the most widely described examples being based on semi-infinite diffusion at planar electrodes.

Descriptions about the effects of alternative electrode geometries are generally restricted to the primary literature (some examples include [1–12]) or more comprehensive monographs [13, 14]. Correction procedures for non-planar diffusion effects have often been reported [1, 3, 5, 9, 15, 16] so that experimental data can be interpreted within the framework of conventional planar diffusion. In one case where optimum conditions for measuring kinetics are described that minimize resistive errors, it was proposed that experimental limits for particular combination of scan rates and electrode sizes are followed to ensure that predominantly planar diffusion is observed [17]. Recognition of the advantages of using smaller electrodes has greatly improved the accuracy of measuring faradaic currents by expert voltammetrists with the influence of non-planar electrode effects being readily incorporated into sophisticated transport models [4, 18–23]. However, these subtleties may be beyond the interest of casual users and a correction method that produces a familiar waveform based on current that can be obtained under conditions that minimize non-faradaic contributions is a valuable tool.

In voltammetry, the concept of converting the measured current into a signal with more desirable properties was

Dedicated to Keith B. Oldham on the occasion of his 80th birthday for his significant contributions to electrochemical science, he is also a generous mentor, colleague, and friend of many.

P. J. Mahon (✉)
Faculty of Life and Social Sciences,
Swinburne University of Technology,
Hawthorn, VIC 3122, Australia
e-mail: pmahon@swin.edu.au

pioneered by Oldham and co-workers [24–32] who demonstrated that the asymmetric peak from a simple voltammogram could be transformed into sigmoidal shaped "neopolarogram" via semiintegration [24, 26–30] or into symmetric peak shaped "derivative neopolarogram" via semidifferentiation [31, 32]. These operations could be performed offline using digital algorithms or hard-wired using analog circuitry between the electrochemical cell and a recording device. This approach is one of few examples where it has been proposed that a "black box" could be incorporated into an electrochemical measurement system. One of the goals of these transformations is to produce a waveform that is more amenable to accurate analysis by removing the time dependence. However, during these transformations of the voltammogram, the unit of the waveform changes and although it can be more reliably analyzed, the analysis requires the use of a slightly different set of relationships between the measured variables.

In experiments where the electrode is very small or the time scale is very large, convergent diffusion enables steady-state conditions to prevail and to produce a sigmoidal shaped voltammogram that is also readily interpreted [33]. A different approach for dealing with the 'mixed' diffusion region where analysis based on either effectively planar or effectively steady-state diffusion is not possible has been proposed and is known as convolutive forecasting [34, 35]. In this procedure, as applied to spherical electrodes, the transient diffusion contribution is corrected enabling a prediction of the steady-state current that would be observed although the experimental time scale is insufficient for pure steady-state diffusion to occur.

In certain circumstances that have been described [36–39], greatly simplified treatments of electrochemical experiments can be achieved because the advent of uniform concentrations of electroactive species at an electrode surface reduces the importance of the spatial coordinate of the electrode and only the transport in the vicinity of the electrode needs to be considered. The theoretical treatment of these systems has been described as semi-analytical because a mathematical solution that captures the time-dependent behavior can be obtained and it is usually in the form of an integral equation, which is then evaluated numerically [40]. Often these integral equations will be in the form of a convolution integral and it has been recognized that there is a generality [36, 37, 41, 42] that relates the current that flows and the concentration of the electroactive species at the electrode surface via a third function that is dependent upon the electrode geometry, any homogeneous chemical reactions, and the diffusion space.

Two convolutions have been described that enable interconversion to occur. The first equation has its origins in semiintegral electroanalysis as developed by Oldham [24–30, 43, 44] and allows the semiintegral, $M(t)$, to be obtained from the current, $I(t)$.

$$M(t) = \frac{\mathrm{d}^{-1/2} I(t)}{\mathrm{d}t^{-1/2}} = I(t) * \frac{1}{\sqrt{\pi t}} \tag{1}$$

The equivalent convolution form was pioneered by Savéant et al. [45–54] and the equivalence occurs because in Laplace space the convolution equation becomes $\overline{I}(s)/\sqrt{s}$, which is also a definition of semiintegration [55] where $\overline{I}(s)$ is the Laplace transform of the current and s is the 'dummy' Laplace variable.

$M(t)$ is directly related to the concentration excursions at the electrode surface for the substrate, S, and product, P, of an electron transfer reaction

$$\mathrm{S}_{\mathrm{soln}} - n\mathrm{e}^- \rightleftharpoons \mathrm{P}_{\mathrm{soln}} \tag{2}$$

where n is the number of electrons transferred between the electrode and the substrate with the sign of n being positive if the reaction is an oxidation and negative for a reduction in accordance with the IUPAC convention for the current. These relationships may be written as

$$\sqrt{D_{\mathrm{S}}}\Delta c_{\mathrm{S}}(t) = \sqrt{D_{\mathrm{P}}}\Delta c_{\mathrm{P}}(t) = \frac{M(t)}{nFA} \tag{3}$$

where F is Faraday's constant, A is the electrode area, D_i is the diffusivity of species i and the concentration excursions, $\Delta c_{\mathrm{S}}(t)$ and $\Delta c_{\mathrm{P}}(t)$, given as the absolute differences

$$\Delta c_i(t) = \left| c_i^{\mathrm{s}}(t) - c_i^{\mathrm{b}} \right| \qquad \text{for } i = \mathrm{S} \text{ or } \mathrm{P} \tag{4}$$

with the superscripts s and b referring to the surface concentrations and bulk concentrations[1] of the electroactive pair, respectively.

The original semiintegral concept strictly applied to uncomplicated electron transfer reactions at planar electrodes but this restriction can be relaxed with the function $1/\sqrt{\pi t}$ in Eq. 1 being replaced by a generalized function, $g(t)$, whose form is dependent on the details of the mechanism and geometry for a particular situation [36–38, 41, 42, 56].

$$M_i(t) = I(t) * g_i(t) \qquad \text{for } i = \mathrm{S} \text{ or } \mathrm{P} \tag{5}$$

In this case, $M(t)$ is described as the *extended semiintegral* [36] because it has all the advantages of the original semiintegration approach but can be extended beyond the restriction of planar electrodes and can also include the influence of coupled chemical reactions. The presence of chemical complications then requires that separate $M(t)$ functions for the substrate and the product to be adopted, namely $M_{\mathrm{S}}(t)$ and $M_{\mathrm{P}}(t)$.

[1] In most cases, P will be initially absent from the solution and the bulk concentration of P will be zero with $\Delta c_{\mathrm{P}}(t) = c_{\mathrm{P}}^{\mathrm{s}}(t)$.

A second convolution enables the current to be defined in terms of the extended semiintegral and the conjugate function of $g(t)$, which has been designated as $h(t)$ with a number of different scenarios having been described [37, 38, 56]

$$I(t) = \frac{\mathrm{d}M_i(t)}{\mathrm{d}t} * h_i(t) = M_i(t) * \frac{\mathrm{d}h_i(t)}{\mathrm{d}t} \quad \text{for } i = \text{S or P} \tag{6}$$

The relationship between $g(t)$ and $h(t)$ is also based on convolution where

$$g_i(t) * h_i(t) = 1 \qquad \text{for } i = \text{S or P} \tag{7}$$

The semi-analytical approach requires that a numerical solution can be obtained and it has been demonstrated [36, 37, 42, 56, 57] that an efficient algorithm developed by Oldham [41], which is amenable for use with evenly time-spaced digitized data, can be used when evaluating convolution integrals.

$$[x(t) * y(t)]_{t=L\Delta} = \frac{1}{\Delta}\left(x_L Y_1 + \sum_{l=1}^{L-1} I_{L-l}(Y_{l-1} - 2Y_l + Y_{l+1})\right) \tag{8}$$

where Δ is a small increment of the total time, x_l and Y_l are used as abbreviations for $x(l\Delta)$ and $Y(l\Delta)$ with

$$Y(t) = \int_0^t \int_0^t y(t)\mathrm{d}t\mathrm{d}t \tag{9}$$

where the capitalized letter is the double integral of a function with a lower case letter.

In this article, a convolutive procedure will be demonstrated that enables voltammograms for various electrode geometries to be reshaped so that the current due to purely planar diffusion can be obtained, which can then be interpreted based on well-established criteria developed for planar electrodes. Examples of five geometries will be considered, this includes the sphere, disk, and cylinder electrodes as well as Nernst diffusion layers, one with an impermeable outer barrier and another where the concentration of electrogenerated species outside the layer is zero, either through reaction or extraction. Also, the convolutive forecasting method will be extended to include the more popular disk electrode geometry.

Theory

Convolutive reshaping

Equations 5 and 6 form the basis for convolutive reshaping. For a particular electrode geometry Eq. 5 can be written using the appropriate $g(t)$ function identified with the subscript E1

$$M(t) = I_{\mathrm{E1}}(t) * g_{\mathrm{E1}}(t) \tag{10}$$

For a second electrode geometry, Eq. 6 would apply using the appropriate $h(t)$ function with subscript E2[2]

$$I_{\mathrm{E2}}(t) = M(t) * \frac{\mathrm{d}h_{\mathrm{E2}}(t)}{\mathrm{d}t} \tag{11}$$

As long as conditions prevail to ensure that $M(t)$ for both electrodes geometries is identical then Eq. 10 can be directly substituted into Eq. 11

$$I_{\mathrm{E2}}(t) = I_{\mathrm{E1}}(t) * g_{\mathrm{E1}}(t) * \frac{\mathrm{d}h_{\mathrm{E2}}(t)}{\mathrm{d}t} \tag{12}$$

This equation can be reduced so that a single convolution based on a specific function that converts from one electrode geometry to another is obtained[3]

$$I_{\mathrm{E2}}(t) = I_{\mathrm{E1}}(t) * \frac{\mathrm{d}p_{\mathrm{E1}\to\mathrm{E2}}(t)}{\mathrm{d}t} = \frac{\mathrm{d}I_{\mathrm{E1}}(t)}{\mathrm{d}t} * p_{\mathrm{E1}\to\mathrm{E2}}(t) \tag{13}$$

where

$$p_{\mathrm{E1}\to\mathrm{E2}}(t) = g_{\mathrm{E1}}(t) * h_{\mathrm{E2}}(t) \tag{14}$$

This is a general result and it should be possible to identify $p(t)$ functions for all combinations of electrodes where $g(t)$ and $h(t)$ functions exist, our immediate interest will be restricted to examples where E2 is a planar electrode with

$$h_{\mathrm{E2}}(t) = \frac{1}{\sqrt{\pi t}} \tag{15}$$

Convolutive forecasting

Spheres and inlaid disk electrodes are the most common geometries where a true steady-state current can be obtained but depending on the electrode size this might occur in a timescale that is unachievable [58]. In practice, an apparent steady-state is only obtained due to the interference of natural convection and often measurements will be obtained in the near steady-state regime where some transient current contribution remains. Zoski and coworkers [34, 35] have developed a procedure that works exactly for spherical electrodes and although it was not theoretically derived for disk electrodes, the procedure was shown to be reasonably successful. It is possible to deduce a general equation for predicting the steady-state current for spheres,

[2] Either form of Eq. 6 can be used but the more direct substitution for $M(t)$ will be demonstrated.

[3] The second form of Eq. 13 is equally valid but it is less preferred when reshaping because it requires the measured current from E1 to be differentiated.

hemispheres and disks from equation (59) of reference [34]. The steady-state current $I_{ss}(t)$ has the same shape as the semiintegral and can therefore be obtained by convolving the current with the appropriate $g(t)$

$$I_{SS}(t) = \frac{2d\sqrt{D}M(t)}{A} = \frac{2d\sqrt{D}}{A} I(t)*g(t) \tag{16}$$

where d is the 'superficial diameter' and A is the area of the sphere, hemisphere or disk used to generate the current.

Spherical electrodes

For a spherical electrode where the diffusion field forms on the external surface, it is known that [41]

$$g_{sph}(t) = \frac{\sqrt{D}}{r_{sph}} \left(\frac{1}{\sqrt{\pi\theta_{sph}}} - \exp(\theta_{sph}) \operatorname{erfc}\left(\sqrt{\theta_{sph}}\right) \right) \tag{17}$$

where r_{sph} is the radius of the sphere, erfc() is the error function complement [59] and the dimensionless time parameter is given by $\theta_{sph} = Dt/r_{sph}^2$. To obtain the $p(t)$ function defined in Eq. 14 it is necessary to find the result of the convolution of Eqs. 15 and 17. This is readily achieved by taking the Laplace transforms of each function, multiply them together to obtain $\overline{p}(s)$ and then find the inverse Laplace transform to obtain $p(t)$. The Laplace transform of $h_{E2}(t)$ from Eq. 15 is $1/\sqrt{s}$ so that for all examples considered here $\overline{p}(s) = \overline{g}(s)/\sqrt{s}$ and the symbolic mathematical capability of Maple was used to perform these transformations[4].

The following reshaping function is obtained

$$p_{sph}(t) = \exp(\theta_{sph}) \operatorname{erfc}\left(\sqrt{\theta_{sph}}\right) \tag{18}$$

In order to apply this function to convert the current obtained at a spherical electrode into the current that would be obtained from a planar electrode, the convolution algorithm described in Eq. 8 is used but requires the double integral of the derivative of $p(t)$ according to Eq. 13. It follows that only the single integral, $P'(t)$, of each $p(t)$ function is necessary to implement the convolution algorithm. For the sphere

$$P'_{sph}(t) = \frac{r_{sph}^2}{D} \left(2\sqrt{\frac{\theta_{sph}}{\pi}} + \exp(\theta_{sph}) \operatorname{erfc}\left(\sqrt{\theta_{sph}}\right) - 1 \right) \tag{19}$$

where $P'_{sph}(t) = \int_0^t p_{sph}(t)\mathrm{d}t$. For convolutive forecasting, the double integral of $g_{sph}(t)$ is required to implement Eq. 16 using the convolution algorithm

$$G_{sph}(t) = \frac{r_{sph}^3}{D^{3/2}} \left(1 - 2\sqrt{\frac{\theta_{sph}}{\pi}} + \theta_{sph} - \exp(\theta_{sph}) \operatorname{erfc}\left(\sqrt{\theta_{sph}}\right) \right) \tag{20}$$

In addition, $d=2\pi r_{sph}$ and $A = 4\pi r_{sph}^2$ for a sphere with $d=\pi r_{sph}$ and $A = 2\pi r_{sph}^2$ for a hemisphere.

Disk electrodes

An overlapping bipartite polynomial series has been obtained for $g_{disk}(t)$ [56, 60]. For small values of θ_{disk}, the five term polynomial is

$$g_{disk}(t) = \frac{\sqrt{D}}{r_{disk}} \sum_{j=1}^{5} a_j \theta_{disk}^{(j-2)/2} \tag{21}$$

where r_{disk} is the radius of the disk electrode and θ_{disk} is the dimensionless time parameter equal to Dt/r_{disk}^2. For large values of θ_{disk}

$$g_{disk}(t) = \frac{\sqrt{D}}{r_{disk}} \left(b_2 \theta_{disk}^{-3/2} + \sum_{j=4}^{8} b_j \theta_{disk}^{(3-2j)/2} \right) \tag{22}$$

with values for a_j and b_j contained in Table 1, the transition occurring at $\theta_{disk}=1.369$.

From these equation the reshaping function for the disk electrode can be obtained and for small values of θ_{disk}

$$p_{disk}(t) = \sum_{j=1}^{5} a_j \theta_{disk}^{(j-1)/2} \tag{23}$$

where values for a_j are listed in Table 1. However, it is not possible to derive the corresponding $p_{disk}(t)$ function for large values of θ_{disk} directly from Eq. 22 but it is necessary to refer to the tabulated coefficients of Aoki and Osteryoung [61]. The original series that was developed is based on a polynomial in Laplace space for $s^{1/2}$ and during the Laplace inversion to obtain a time-dependent series, the integer powers of s disappear resulting in a polynomial without integer powers. If we recall that $\overline{p}(s) = \overline{g}(s)/\sqrt{s}$ then in effect, the alternate terms that disappeared when obtaining $g(t)$ become the terms in the series for $p(t)$

$$p_{disk}(t) = b_1 \theta_{disk}^{1/2} + \sum_{j=3}^{7} b_j \theta_{disk}^{(3-2j)/2} \tag{24}$$

with values for b_j given in Table 1. The transition from Eq. 23 to Eq. 24 should occur at $\theta_{disk}=1.557$. The following

[4] As noted earlier, when $1/\sqrt{\pi t}$ is the convolving function, as it is here for $h_{E2}(t)$ with these examples, then the resulting $p(t)$ functions are the semiintegral of the corresponding $g(t)$ functions and is possible to use tabulated semiintegrals [44] to achieve the same result.

Table 1 A list of polynomial coefficients for functions describing the properties of the disk electrode

j	*g(t)*		*G(t)*		*p(t)*		*P'(t)*	
	a_j	b_j	a_j	b_j	a_j	b_j	a_j	b_j
1	$1/\pi^{1/2}$	0	$4/3\pi^{1/2}$	$\pi/4$	1	$\pi^{1/2}/4$	1	$\pi^{1/2}/2$
2	−1	$1/4\pi^{1/2}$	$-1/2$	$-1/\pi^{1/2}$	$-2/\pi^{1/2}$	0	$-4/3\pi^{1/2}$	$-1/2$
3	$3/2\pi^{1/2}$	0	$2/5\pi^{1/2}$	0.21682	3/4	-7.3852×10^{-2}	3/8	0.14770
4	−0.38472	-4.7016×10^{-2}	-6.4120×10^{-2}	-6.2688×10^{-2}	−0.28941	1.4770×10^{-2}	−0.11576	-9.8469×10^{-3}
5	7.7365×10^{-2}	4.7014×10^{-3}	8.8417×10^{-3}	1.2537×10^{-3}	5.1422×10^{-2}	4.2050×10^{-3}	1.7141×10^{-2}	-1.6820×10^{-3}
6		1.5597×10^{-2}		1.7826×10^{-3}		-9.5018×10^{-3}		1.7826×10^{-3}
7		-1.9504×10^{-2}		-1.2384×10^{-3}		6.5378×10^{-3}		-1.4526×10^{-3}
8		5.7178×10^{-3}		2.3102×10^{-4}				

Series expansion using Maple has resulted in different values for the *b* coefficients of terms 5–8 for *g*(*t*) and *G*(*t*) compared with reference [56]. A comparison shows that these changes have not significantly altered the results for *g*(*t*) and *G*(*t*) but a small adjustment of the transition point is necessary and is given in the main text

two series enable the convolution algorithm to be applied for convolutive reshaping, for small values of θ_{disk}

$$P'_{\text{disk}}(t) = \frac{r^2_{\text{disk}}}{D}\sum_{j=1}^{5} a_j \theta_{\text{disk}}^{(j+1)/2} \tag{25}$$

and for large values of θ_{disk}

$$P'_{\text{disk}}(t) = \frac{r^2_{\text{disk}}}{D}\left(b_1\theta_{\text{disk}}^{1/2} + b_2 + \sum_{j=3}^{7} b_j \theta_{\text{disk}}^{(5-2j)/2}\right) \tag{26}$$

where the values for a_j and b_j are listed in Table 1 and the transition occurring at θ_{disk}=1.557.

The algorithm to implement convolutive forecasting for the disk requires the following double integrals, for small values of θ_{disk}

$$G_{\text{disk}}(t) = \frac{r^3_{\text{disk}}}{D^{3/2}}\sum_{j=1}^{5} a_j \theta_{\text{disk}}^{(j+2)/2} \tag{27}$$

and for large values of θ_{disk}

$$G_{\text{disk}}(t) = \frac{r^3_{\text{disk}}}{D^{3/2}}\left(\sum_{j=1}^{3} b_j \theta_{\text{disk}}^{(3-j)/2} + \sum_{j=4}^{8} b_j \theta_{\text{disk}}^{(7-2j)/2}\right) \tag{28}$$

with values for a_j and b_j contained in Table 1 and the transition occurring at θ_{disk}=1.554. In addition, $d=2r_{\text{disk}}$ and $A = \pi r^2_{\text{disk}}$ for the disk.

Cylindrical electrodes

Unlike the spherical and disk geometries, an expression for $g_{\text{cyl}}(t)$ doesn't exist that is applicable for all times. For small values of the dimensionless time parameter θ_{cyl}, which is equal to Dt/r^2_{cyl} with r_{cyl} being the radius of a cylinder; an asymptotic series expansion has been determined [36]

$$g_{\text{cyl}}(t) = \frac{\sqrt{D}}{r_{\text{sph}}}\left(\frac{1}{\sqrt{\pi\theta_{\text{cyl}}}} - \frac{1}{2} + \frac{3}{4}\sqrt{\frac{\theta_{\text{cyl}}}{\pi}} - \frac{3\theta_{\text{cyl}}}{8} + \ldots\right) \tag{29}$$

This can be used to obtain the reshaping function for a cylinder

$$p_{\text{cyl}}(t) = 1 - \sqrt{\frac{\theta_{\text{cyl}}}{\pi}} + \frac{3\theta_{\text{cyl}}}{8} - \frac{\theta^{3/2}_{\text{cyl}}}{2\sqrt{\pi}} + \ldots \tag{30}$$

which is implemented as the following integral

$$P'_{\text{cyl}}(t) = \frac{r^2_{\text{cyl}}}{D}\left(\theta_{\text{cyl}} - \frac{2\theta^{3/2}_{\text{cyl}}}{3\sqrt{\pi}} + \frac{3\theta^2_{\text{cyl}}}{16} - \frac{\theta^{5/2}_{\text{cyl}}}{5\sqrt{\pi}} + \ldots\right) \tag{31}$$

For large values of θ_{cyl}, a series expansion for $g_{\text{cyl}}(t)$ can obtained from the derivative of the $\Phi(\theta_{\text{cyl}})$ function presented by Aoki et al. [62] that is used to predict the chronopotentiometric response for cylindrical electrodes, they also presented the series for small values of θ_{cyl}, which is identical to Eq. 29 after differentiation. The resulting equation is

$$g_{\text{cyl}}(t) = \frac{\sqrt{D}}{r_{\text{sph}}}\left(\frac{1}{2\theta_{\text{cyl}}} - \frac{\ln(4\theta_{\text{cyl}}) - \gamma}{4\theta^2_{\text{cyl}}} + \frac{4 + \pi^2 + 4(\ln(4\theta_{\text{cyl}}) - \gamma) - 6(\ln(4\theta_{\text{cyl}}) - \gamma)^2}{32\theta^3_{\text{cyl}}} + \ldots\right) \tag{32}$$

where γ is Euler's constant (0.57721...). In this case the reshaping function is

$$p_{\text{cyl}}(t) = \frac{\ln(16\theta_{\text{cyl}}) - \gamma}{2\sqrt{\pi\theta_{\text{cyl}}}} + \frac{4 + \pi^2 + 4(\ln(16\theta_{\text{cyl}}) - \gamma) - 2(\ln(16\theta_{\text{cyl}}) - \gamma)^2}{32\sqrt{\pi}\theta^{3/2}_{\text{cyl}}} + \ldots \tag{33}$$

The intermediate region between these two series for small and large values of θ_{cyl} can obtained by numerical

integration and Aoki et al. [62] developed an empirical equation for $\Phi(\theta_{cyl})$ that is suitable for all times with minor error. However, the presence of an $\exp\left(-\sqrt{\theta_{cyl}}\right)$ term in their empirical equation results in a complexity created by the transform procedures that is not easily implemented. This problem is best avoided by developing separate empirical equations based on the series solutions listed above similar to the way that $\Phi(\theta_{cyl})$ was developed by Aoki et al. but this has not been attempted here.

Nernst diffusion layer with an impermeable outer barrier

For this electrode geometry, the electrode surface is a plane that is uniformly accessible but once the diffusion layer extends to the width of the solution between the electrode and the barrier, the diffusion field becomes distorted because the electroactive species is not replenished as it would be in the absence of the barrier. This depletion effect results in voltammograms whose shape is dependent on the time scale and solution layer thickness [63].

The $g(t)$ function for this configuration is known [36, 41]

$$g_{ndb}(t) = \frac{\sqrt{D}}{\delta_{nbd}}\theta_3(0;\theta_{ndb}) \tag{34}$$

where δ_{ndb} is the thickness of the solution layer, θ_{ndb} is the dimensionless time parameter equal to Dt/δ_{ndb}^2 and $\theta_3(0;\ \theta_{ndb})$ is the theta-3 function of zero parameter [59]. The theta-3 function can be expressed in two forms that are both highly convergent [59], for smaller values of θ_{ndb}

$$\theta_3(0;\theta_{ndb}) = \frac{1}{\sqrt{\pi\theta_{ndb}}}\left[1 + 2\sum_{j=1}^{\infty}\exp\left(\frac{-j^2}{\theta_{ndb}}\right)\right] \tag{35}$$

and from this equation, $p_{ndb}(t)$ is obtained

$$p_{ndb}(t) = 1 + 2\sum_{j=1}^{\infty}\mathrm{erfc}\left(\frac{j}{\sqrt{\theta_{ndb}}}\right) \tag{36}$$

with the corresponding integral used in the convolution algorithm

$$P'_{ndb}(t) = \frac{\delta_{ndb}^2}{D}\left[\theta_{ndb} + 2\sum_{j=1}^{\infty}\left(\theta_{ndb}\mathrm{erfc}\left(\frac{j}{\sqrt{\theta_{ndb}}}\right) - 2j\sqrt{\frac{\theta_{ndb}}{\pi}}\exp\left(\frac{-j^2}{\theta_{ndb}}\right) - 2j^2\mathrm{erf}\left(\frac{j}{\sqrt{\theta_{ndb}}}\right)\right)\right] \tag{37}$$

For larger values of θ_{ndb}

$$\theta_3(0;\theta_{ndb}) = 1 + 2\sum_{j=1}^{\infty}\exp\left(-j^2\pi^2\theta_{ndb}\right) \tag{38}$$

and from this equation, $p_{ndb}(t)$ is obtained

$$p_{ndb}(t) = 2\sqrt{\frac{\theta_{ndb}}{\pi}} + \frac{4}{\pi^{3/2}}\sum_{j=1}^{\infty}\frac{\mathrm{daw}\left(j\pi\sqrt{\theta_{ndb}}\right)}{j} \tag{39}$$

where daw() is Dawson's Integral [59], with the corresponding integral used in the convolution algorithm being

$$P'_{ndb}(t) = \frac{\delta_{ndb}^2}{D}\left[\frac{4\theta_{ndb}^{3/2}}{3\sqrt{\pi}} + \frac{4}{\pi^{5/2}}\sum_{j=1}^{\infty}\left(\frac{\sqrt{\theta_{ndb}}}{j^2} - \frac{\mathrm{daw}\left(j\pi\sqrt{\theta_{ndb}}\right)}{j^3\pi}\right)\right] \tag{40}$$

Nernst diffusion layer with an open boundary

For this electrode geometry, the diffusion occurs in a finite space but beyond this region the concentration of the electroactive species remains constant and a membrane covered electrode is a typical example. In this case, the electroactive species is replenished at a greater rate than would occur if there was no boundary. This geometry has been considered previously and the $g(t)$ function is known [36, 41]

$$g_{ndo}(t) = \frac{\sqrt{D}}{\delta_{nbo}}\theta_2(0;\theta_{ndo}) \tag{41}$$

where δ_{ndo} is the thickness of the solution layer, θ_{ndo} is the dimensionless time parameter equal to Dt/δ_{ndo}^2 and $\theta_2(0;\ \theta_{ndo})$ is the theta-2 function of zero parameter [59]. The theta-2 function can also be expressed as two series [59], for small values of θ_{ndo}

$$\theta_2(0;\theta_{ndo}) = \frac{1}{\sqrt{\pi\theta_{ndo}}}\left[1 + 2\sum_{j=1}^{\infty}(-)^j\exp\left(\frac{-j^2}{\theta_{ndo}}\right)\right] \tag{42}$$

from which $p_{ndo}(t)$ is obtained

$$p_{ndo}(t) = 1 + 2\sum_{j=1}^{\infty}(-)^j\mathrm{erfc}\left(\frac{j}{\sqrt{\theta_{ndo}}}\right) \tag{43}$$

and the integral required for the convolution algorithm is

$$P'_{ndo}(t) = \frac{\delta_{ndo}^2}{D}\left[\theta_{ndo} + 2\sum_{j=1}^{\infty}(-)^j\left(\theta_{ndo}\mathrm{erfc}\left(\frac{j}{\sqrt{\theta_{ndo}}}\right) - 2j\sqrt{\frac{\theta_{ndo}}{\pi}}\exp\left(\frac{-j^2}{\theta_{ndo}}\right) - 2j^2\mathrm{erf}\left(\frac{j}{\sqrt{\theta_{ndo}}}\right)\right)\right] \tag{44}$$

For larger values of θ_{ndo}

$$\theta_2(0;\theta_{ndo}) = 2\sum_{j=0}^{\infty}\exp\left(-\left(j+\tfrac{1}{2}\right)^2\pi^2\theta_{ndo}\right) \tag{45}$$

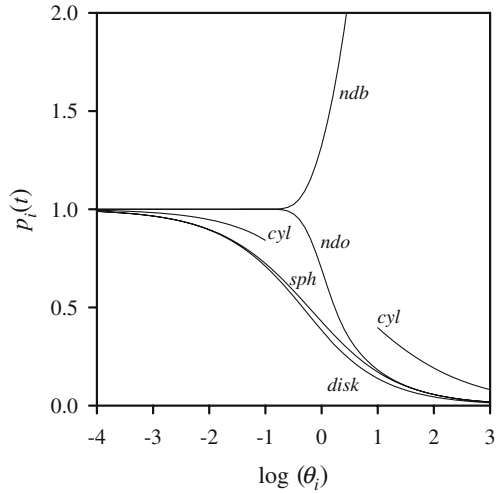

Fig. 1 A comparison of the various $p(t)$ functions that have been developed for the described examples where the labels on the graph correspond to the subscript i

and from this equation, $p_{ndo}(t)$ is obtained

$$p_{ndo}(t) = \frac{4}{\pi^{3/2}} \sum_{j=0}^{\infty} \mathrm{daw}\left(\left(j+\tfrac{1}{2}\right)\pi\sqrt{\theta_{ndb}}\right) \tag{46}$$

with the corresponding integral used in the convolution algorithm being

$$P'_{ndo}(t) = \frac{\delta_{ndo}^2}{D}\left[\frac{4}{\pi^{5/2}} \sum_{j=0}^{\infty}\left(\frac{\sqrt{\theta_{ndo}}}{\left(j+\tfrac{1}{2}\right)^2} - \frac{\mathrm{daw}\left(\left(j+\tfrac{1}{2}\right)\pi\sqrt{\theta_{ndo}}\right)}{\left(j+\tfrac{1}{2}\right)^3\pi}\right)\right] \tag{47}$$

Results

The convolutive reshaping function for the five electrode geometries are displayed in Fig. 1. For small values of the various dimensionless time parameters it can be seen that all the $p(t)$ functions approach unity. Clearly at this limit, all electrode responses are dominated by planar diffusion and if we consider the second form of Eq. 13 as $p(t)\rightarrow 1$ then the convolution results in integration and the current is unchanged.

$$I_{E2}(t) = \frac{\mathrm{d}I_{E1}(t)}{\mathrm{d}t} * 1 = I_{E1}(t) \tag{48}$$

For large θ, values of $p(t)$ less than one correspond to an enhanced current being obtained relative to what would be observed for a planar electrode. In one of the examples, values greater than one occur for a Nernst diffusion layer where the concentration of the electroactive species becomes depleted compared to unimpeded diffusion and in this case the observed current needs to be amplified to obtain the appropriate planar current.

Examples

All five geometries that have been described can be simulated using DigiElch (http://www.digielch.de) [64–68] and convolutive reshaping was applied to a number of simulated voltammograms. Direct comparison with simulated voltammograms obtained at a planar electrode of equal area was performed as a test of the reshaping procedure. Convolutive forecasting was also applied to simulated voltammograms obtained from spherical and disk electrodes with the resulting voltammograms compared with the predicted steady-state current [33, 34]

$$I_{SS}(t) = \frac{2dnFDc_S^b}{1+\exp\left(\frac{nF(E^o-E(t))}{RT}\right)} \tag{49}$$

Figure 2 presents results obtained for both convolutive reshaping and convolutive forecasting applied to a voltammogram obtained for a spherical electrode under conditions where mixed diffusion is prevalent. From the original voltammogram, the planar component has been derived using convolutive reshaping and it is directly compared to a simulated voltammogram obtained for a planar electrode of the same area. An exact correspondence is found from the comparison. A noteworthy aspect for this mixed diffusion situation is that the peak separation, which is a well-established criteria for determining electrochemical reversibility [69], is much greater than the peak separation that occurs for purely planar diffusion. Although the electrode reaction is reversible, the peak separation varies with

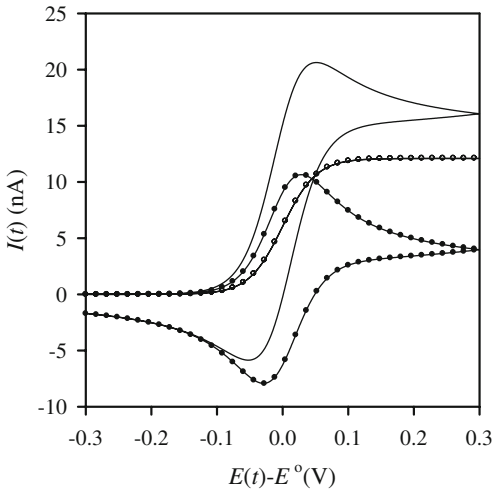

Fig. 2 The *single line* is a simulated voltammogram obtained for a spherical electrode using the following parameters r_{sph}=10 μm, $D = 1\times10^{-5}$ cm^2 s^{-1}, c_S^b = 1mM and scan rate=1 V s^{-1}. The *solid circles* are for a simulated voltammogram obtained for a planar electrode of equal area to the spherical electrode and are superimposed on the voltammogram resulting from convolutive reshaping. The *open circles* are calculated from Eq. 49 and are superimposed on the voltammogram resulting from convolutive forecasting

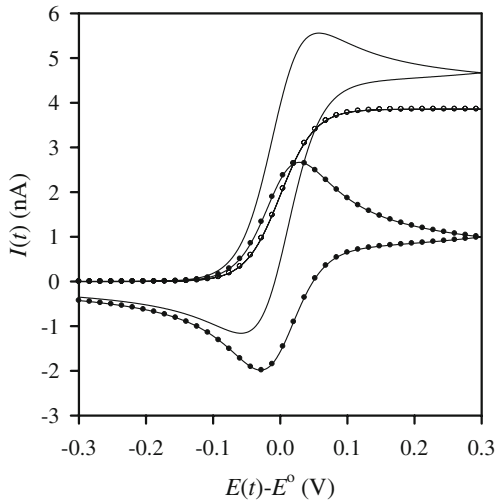

Fig. 3 The *single line* is a simulated voltammogram obtained for a disk electrode using the following parameters r_{disk}=10 μm, $D = 1 \times 10^{-5}$ cm^2 s^{-1}, $c_S^b = 1$mM and scan rate=1 V s^{-1}. The *solid circles* are for a simulated voltammogram obtained for a planar electrode of equal area to the disk electrode and are superimposed on the voltammogram resulting from convolutive reshaping. The *open circles* are calculated from Eq. 49 and are superimposed on the voltammogram resulting from convolutive forecasting

changes in scan rate for a given electrode size in the mixed diffusion regime whereas the test for reversibility with planar diffusion is for the peak separation to be independent of scan rate. The influence of mixed diffusion on the properties of voltammograms obtained using non-planar electrodes is well known but convolutive reshaping provides a straightforward way for quickly assessing reversibility without the need to consult graphs or tables

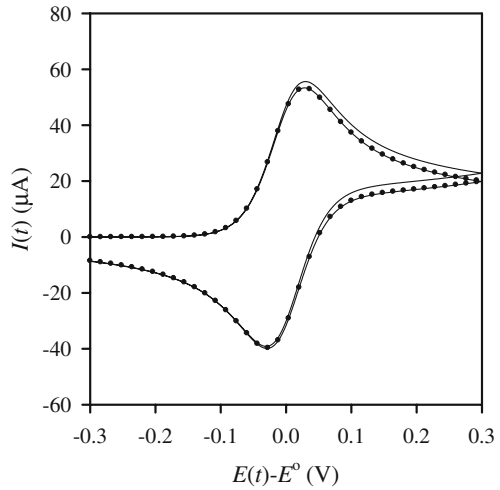

Fig. 4 The *single line* is a simulated voltammogram obtained for a cylindrical electrode using the following parameters r_{cyl}=100 μm, cylinder length=1 cm, $D = 1 \times 10^{-5}$ cm^2 s^{-1}, $c_S^b = 1$mM and scan rate=1 V s^{-1}. The *solid circles* are for a simulated voltammogram obtained for a planar electrode of equal area to the cylindrical electrode and are superimposed on the voltammogram resulting from convolutive reshaping

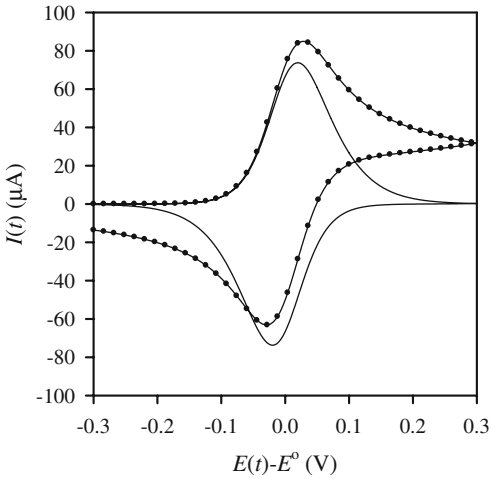

Fig. 5 The *single line* is a simulated voltammogram obtained for a Nernst diffusion layer with an impermeable outer barrier using the following parameters δ_{ndb}=100 μm, A_{ndb}=1 cm^2, $D = 1 \times 10^{-5}$ cm^2 s^{-1}, $c_S^b = 1$mM and scan rate=0.01 V s^{-1}. The *solid circles* are for a simulated voltammogram obtained for a planar electrode with an area equal to A_{ndb} and are superimposed on the voltammogram resulting from convolutive reshaping

[4, 70, 71] that contain condition specific peak values. The steady-state response has also been obtained from the original voltammogram using convolutive forecasting and direct comparison with Eq. 49 demonstrates the effectiveness of this transformation.

Results for the disk electrode are presented in Fig. 3. It is known the current obtained for a spherical electrode is the sum of the planar and steady-state currents; and that the current for a disk electrode has other time-dependent

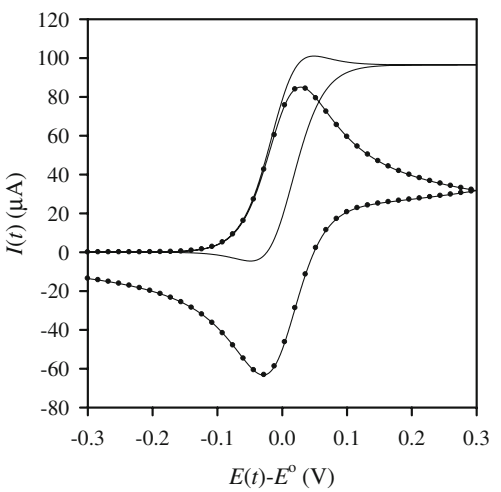

Fig. 6 The *single line* is a simulated voltammogram obtained for a Nernst diffusion layer with an open boundary using the following parameters δ_{ndo}=100 μm, A_{ndo}=1 cm^2, $D = 1 \times 10^{-5}$ cm^2 s^{-1}, $c_S^b =$ 1mM and scan rate=0.01 V s^{-1}. The *solid circles* are for a simulated voltammogram obtained for a planar electrode with an area equal to A_{ndo} and are superimposed on the voltammogram resulting from convolutive reshaping

components. This is clearly demonstrated from Figs. 2 and 3 where the separate planar and steady-state components that have been directly obtained from a single voltammogram are shown.

The limitation of only being able to use the small θ_{cyl} series equation for $p_{cyl}(t)$ restricts the range of application for convolutive reshaping but it is clear from Fig. 4 that the general principles are still valid. The example of the Nernst diffusion layer with an impermeable outer barrier is shown in Fig. 5 and in this case the peak separation is intermediate between that expected for predominantly planar diffusion and no separation, which is the limiting behavior for a very thin layer between the electrode and the barrier. Convolutive reshaping results in an increased current and gives a peak separation that would have been obtained if diffusion was unimpeded. A vastly different shaped voltammogram is obtained for the example of the Nernst diffusion layer with an open boundary as displayed in Fig. 6 and convolutive reshaping enables the planar diffusion current to be obtained.

In all cases, convolutive reshaping has been able to obtain the reversible voltammogram that is due to planar diffusion. However, it should be noted that the analysis of any departure from reversible electrode kinetics based on the criteria developed for planar electrodes may introduce some error. This is because of the restriction involved in the development of Eq. 13, which is that the surface concentration of the substrate (and therefore product) must be identical for both electrode geometries and reversibility is one circumstance that satisfies this restriction. It would be expected that a full quantitative analysis based on the original measured currents using direct analysis methods, such as Global Analysis [57, 72–74], or comparisons with modelling obtained from simulations containing the appropriate geometry, such as DigiElch, is required to obtain an accurate assessment of any experimental data.

Conclusion

A new convolutive procedure for obtaining the planar diffusion component from a voltammogram has been described and demonstrated for a variety of diverse examples. A major advantage of convolutive reshaping is that a voltammogram that is more readily interpreted is the result. A related procedure that has previously been developed for spherical electrodes, known as convolutive forecasting, has been extended so that an exact treatment of disk electrodes is now possible. Using established criteria, an initial assessment of the resulting steady-state voltammogram can be quickly obtained as a convenient alternative to the use of sophisticated simulation procedures that are required when mixed diffusion conditions are encountered. However, the proposed methods do not replace more rigorous sophisticated analysis procedures which will always be required for accurate quantitative evaluation of experimental voltammetric data.

References

1. Reinmuth WH (1957) J Am Chem Soc 79:6358. doi:10.1021/ja01581a004
2. Oldham KB (1973) J Electroanal Chem 41:351. doi:10.1016/S0022-0728(73)80413-9
3. Brydon GA, Oldham KB (1981) J Electroanal Chem 122:353
4. Heinze J (1981) Ber Bunsen-Ges. Phys Chem Chem Phys 85:1096
5. Goodisman J (1983) J Electroanal Chem 144:33. doi:10.1016/S0022-0728(83)80141-7
6. Aoki K, Akimoto K, Tokuda K, Matsuda H, Osteryoung J (1984) J Electroanal Chem 171:219. doi:10.1016/0022-0728(84)80115-1
7. Aoki K, Honda K, Tokuda K, Matsuda H (1985) J Electroanal Chem 182:267. doi:10.1016/0368-1874(85)87005-2
8. Frankenthal RP, Shain I (1956) J Am Chem Soc 78:2969. doi:10.1021/ja01594a013
9. Olmstead ML, Nicholson RS (1967) J Electroanal Chem 14:133. doi:10.1016/0022-0728(67)80063-9
10. Oldham KB (1981) J Electroanal Chem 122:1. doi:10.1016/s0022-0728(81)80136-2
11. Myland JC, Oldham KB (1983) J Electroanal Chem 147:295. doi:10.1016/S0022-0728(83)80074-6
12. Cope DK (1997) J Electroanal Chem 439:7. doi:10.1016/S0022-0728(97)00367-7
13. Oldham KB, Myland JC (1994) Fundamentals of electrochemical science. Academic, San Diego
14. Bard AJ, Faulkner LR (2000) Electrochemical methods: fundamentals and applications. Wiley, New York
15. Bond AM, Oldham KB (1983) J Electroanal Chem 158:193. doi:10.1016/S0022-0728(83)80608-1
16. Myland JC, Oldham KB (1985) J Electroanal Chem 185:29. doi:10.1016/0368-1874(85)85839-1
17. Bowyer WJ, Engelman EE, Evans DH (1989) J Electroanal Chem 262:67. doi:10.1016/0022-0728(89)80012-9
18. Shoup D, Szabo A (1982) J Electroanal Chem 140:237. doi:10.1016/0022-0728(82)85171-1
19. Michael AC, Wightman RM, Amatore CA (1989) J Electroanal Chem 267:33. doi:10.1016/0022-0728(89)80235-9
20. Amatore CA, Fosset B (1992) J Electroanal Chem 328:21. doi:10.1016/0022-0728(92)80167-3
21. Gavaghan DJ (1998) J Electroanal Chem 456:13. doi:10.1016/S0022-0728(98)00226-5
22. Gavaghan DJ (1998) J Electroanal Chem 456:25. doi:10.1016/S0022-0728(98)00233-2
23. Gillow K, Gavaghan DJ, Suli E (2006) J Electroanal Chem 587:1. doi:10.1016/j.jelechem.2005.09.028
24. Grenness M, Oldham KB (1972) Anal Chem 44:1121. doi:10.1021/ac60315a037
25. Oldham KB (1972) Anal Chem 44:196. doi:10.1021/ac60309a028
26. Goto M, Oldham KB (1973) Anal Chem 45:2043. doi:10.1021/ac60334a027
27. Oldham KB (1973) Anal Chem 45:39. doi:10.1021/ac60323a005
28. Goto M, Oldham KB (1974) Anal Chem 46:1522. doi:10.1021/ac60347a058
29. Goto M, Oldham KB (1976) Anal Chem 48:1671. doi:10.1021/ac50006a012
30. Oldham KB (1976) J Electroanal Chem 72:371. doi:10.1016/S0022-0728(76)80323-3

31. Dalrymple-Alford P, Goto M, Oldham KB (1977) J Electroanal Chem 85:1. doi:10.1016/S0022-0728(77)80148-4
32. Dalrymple-Alford P, Goto M, Oldham KB (1977) Anal Chem 49:1390. doi:10.1021/ac50017a025
33. Bond AM, Oldham KB, Zoski CG (1989) Anal Chim Acta 216:177. doi:10.1016/S0003-2670(00)82009-7
34. Zoski CG, Bond AM, Colyer CL, Myland JC, Oldham KB (1989) J Electroanal Chem 263:1. doi:10.1016/0022-0728(89)80120-2
35. Zoski CG, Gu C (2000) J Electroanal Chem 480:106. doi:10.1016/S0022-0728(99)00453-2
36. Mahon PJ, Oldham KB (1998) J Electroanal Chem 445:179. doi:10.1016/S0022-0728(97)00535-4
37. Mahon PJ, Oldham KB (1999) J Electroanal Chem 464:1. doi:10.1016/S0022-0728(98)00450-1
38. Mahon PJ, Oldham KB (2001) Electrochim Acta 46:953. doi:10.1016/S0013-4686(00)00680-0
39. Mahon PJ, Oldham KB (2006) J Solid State Electrochem 10:785. doi:10.1007/s10008-006-0169-0
40. Myland JC, Oldham KB (2004) J Electroanal Chem 568:101. doi:10.1016/j.jelechem.2004.01.010
41. Oldham KB (1986) Anal Chem 58:2296. doi:10.1021/ac00124a040
42. Mahon PJ, Myland JC, Oldham KB (2002) J Electroanal Chem 537:1. doi:10.1016/S0022-0728(02)01263-9
43. Oldham KB, Zoski CG (1983) J Electroanal Chem 145:265. doi:10.1016/s0022-0728(83)80086-2
44. Oldham KB (1997) J Electroanal Chem 430:1. doi:10.1016/S0022-0728(96)04827-9
45. Saveant JM, Vianello E (1967) Electrochim Acta 12:1545. doi:10.1016/0013-4686(67)80070-7
46. Saveant JM, Vianello E (1967) Electrochim Acta 12:629. doi:10.1016/0013-4686(67)85031-X
47. Mastragostino M, Nadjo L, Saveant JM (1968) Electrochim Acta 13:721. doi:10.1016/0013-4686(68)85007-8
48. Ammar F, Saveant JM (1973) J Electroanal Chem 47:215. doi:10.1016/S0022-0728(73)80448-6
49. Imbeaux JC, Saveant JM (1973) J Electroanal Chem 44:169. doi:10.1016/S0022-0728(73)80244-X
50. Nadjo L, Saveant JM, Tessier D (1974) J Electroanal Chem 52:403. doi:10.1016/S0022-0728(74)80450-X
51. Saveant JM, Tessier D (1975) J Electroanal Chem 65:57. doi:10.1016/S0022-0728(75)80055-6
52. Saveant JM, Tessier D (1975) J Electroanal Chem 61:251. doi:10.1016/S0022-0728(75)80226-9
53. Saveant JM, Tessier D (1977) J Electroanal Chem 77:225. doi:10.1016/S0022-0728(77)80474-9
54. Amatore C, Nadjo L, Saveant JM (1978) J Electroanal Chem 90:321. doi:10.1016/S0022-0728(78)80069-2
55. Oldham KB, Spanier J (1974) The fractional calculus. Academic, New York
56. Mahon PJ, Oldham KB (2004) Electrochim Acta 49:5049. doi:10.1016/j.electacta.2004.07.018
57. Zoski CG, Oldham KB, Mahon PJ, Henderson TLE, Bond AM (1991) J Electroanal Chem 297:1. doi:10.1016/0022-0728(91)85355-S
58. Zoski CG, Bond AM, Allinson ET, Oldham KB (1990) Anal Chem 62:37. doi:10.1021/ac00200a008
59. Spanier J, Oldham KB (1987) An atlas of functions. Hemisphere, Washington
60. Mahon PJ, Oldham KB (2004) Electrochim Acta 49:5041. doi:10.1016/j.electacta.2004.06.005
61. Aoki K, Osteryoung J (1984) J Electroanal Chem 160:335. doi:10.1016/s0022-0728(84)80136-2
62. Aoki K, Honda K, Tokuda K, Matsuda H (1985) J Electroanal Chem 195:51. doi:10.1016/0022-0728(85)80004-8
63. Aoki K, Tokuda K, Matsuda H (1983) J Electroanal Chem 146:417. doi:10.1016/S0022-0728(83)80601-9
64. Rudolph M (1992) J Electroanal Chem 338:85. doi:10.1016/0022-0728(92)80415-Z
65. Rudolph M (2004) J Electroanal Chem 571:289. doi:10.1016/j.jelechem.2004.05.017
66. Rudolph M (2005) J Comput Chem 26:1193. doi:10.1002/jcc.20256
67. Rudolph M (2005) J Comput Chem 26:619. doi:10.1002/jcc.20200
68. Rudolph M (2005) J Comput Chem 26:633. doi:10.1002/jcc.20201
69. Nicholson RS (1965) Anal Chem 37:1351. doi:10.1021/ac60230a016
70. Neudeck A, Dittrich J (1991) J Electroanal Chem 313:37. doi:10.1016/0022-0728(91)85170-T
71. Lavagnini I, Pastore P, Magno F (1992) J Electroanal Chem 333:1. doi:10.1016/0022-0728(92)80377-G
72. Bond AM, Henderson TLE, Oldham KB (1985) J Electroanal Chem 191:75. doi:10.1016/S0022-0728(85)80006-1
73. Bond AM, Mahon PJ, Maxwell EA, Oldham KB, Zoski CG (1994) J Electroanal Chem 370:1. doi:10.1016/0022-0728(93)03162-I
74. Bond AM, Mahon PJ, Oldham KB, Zoski CG (1994) J Electroanal Chem 366:15. doi:10.1016/0022-0728(93)02707-O